On block iterative correction in strongly coupled data assimilation

M. Yaremchuk*[1], C. Beattie[2], and S. Frolov[3]

[1]*Naval Research Laboratory, Stennis Space Center, MS, USA*
[2] *Department of Mathematics, Virginia Tech, VA, USA*
[3] *CIRES, University of Colorado Boulder, CO, USA*

*Correspondence to: Naval Research Laboratory,1009 Balch Blvd., Stennis Space Center, 39522, MS, USA. E-mail: max.yaremchuk@nrlssc.navy.mil

The on-going transition to coupled data assimilation (DA) systems encounters substantial technical difficulties associated with the need to merge together different elements of atmospheric and ocean DA systems that typically have had independent development paths for decades. In this study we consider the incorporation of strong coupling in the observation space via successive corrections that involve the application of only uncoupled solvers to a sequence of innovation vectors. The coupled increment is then obtained by projecting a coupled innovation vector on the grid using coupled ensemble correlations. Proposed approach is motivated by the classic block Jacobi matrix iteration applied to the coupled system using the uncoupled solvers as a preconditioner. The method is tested via numerical experiments with the CERA ensemble in a simplified setting.

Key Words: strongly coupled data assimilation; coupled modeling; iterative methods

Received . . .

1. Introduction

As numerical weather prediction centers move towards the implementation of strongly coupled ocean-atmosphere models to form the dynamical cores of their forecasting systems (Rabier (2005); Bauer et al (2015)), there is growing interest in transitioning the associated data assimilation (DA) schemes into compatible strongly coupled regimes (Smith et al (2015), Penny et al (2017), Zhang et al (2020)), which utilizes the coupled error covariances for updating the state of the coupled system. This transition is hindered both by theoretical challenges, e.g., consistent estimation of background error covariances between the two fluids (Frolov et al (2016); Smith et al (2017) Smith et al (2018)), as well as by practical challenges associated with the integration of two separate DA systems into a single entity.

Currently, several strategies for incorporating strongly coupled DA approaches into operational forecasting are being explored. Laloyaux et al (2016) proposed iterative updates of the coupled atmosphere-ocean increment in order to synchronize the flow of information between two otherwise uncoupled DA systems. In this approach, a sequence of background model trajectories is produced by coupled model runs, but increments for every iterate are computed separately for ocean and atmosphere components, using the existing uncoupled DA systems. The approach bypasses the above mentioned technical difficulty of transferring the DA system into the strongly coupled regime at the expense of performing multiple coupled model runs. In a series of idealized numerical experiments, Laloyaux et al (2018) have shown that the coupled increments obtained after several iterations of the outer loop provide better approximation of the fully coupled first guess trajectory as compared to the case when only one iteration was performed which produced a weakly balanced first guess trajectory (Smith et al (2015); Lea et al (2015)). As a result, this approach has the potential of reducing initialization shocks in coupled forecasts through better accounting of ocean-atmosphere interactions within the assimilation window.

Another way to approximate the fully-coupled DA system within the hybrid ensemble-variational approach is to specify the coupled error cross-covariances using the localized sample covariances. This approach requires, among other things, careful localization of the ensemble covariances at the ocean-atmosphere interface, since limitations in ensemble size can introduce significant sampling noise in estimating the cross-correlations between the fluids whose dynamics is characterized by different spatio-temporal scales. Implementation of this "direct" approach within an operational forecasting framework presents a large number of other technical challenges as well (Frolov et al (2016); Sluka et al (2016); Wada et al (2017)).

In particular, Frolov et al (2016) proposed to reduce the above strongly coupled ocean-atmosphere system to the block-wise solution of two smaller systems of equations with the approximate sizes of the atmospheric and oceanic innovation vectors. Although these problems can be solved in parallel and much faster than the strongly coupled one, a variety of technical difficulties associated with merging the atmospheric and oceanic solvers within the respective boundary layers remain in place.

 Prepared using qjrms4.cls *[Version: 2013/10/14 v1.1]*

In this paper we show that these difficulties can be bypassed by approaching the strongly coupled solution through a process of iterative correction of the uncoupled solution utilizing (already existing) uncoupled solvers. In the following sections, we provide a brief account of the method of Frolov et al (2016), then describe our proposed iterative approach, provide results of the numerical testing, and finally discuss some perspectives and potential enhancements.

2. The strongly coupled DA problem

Correct specification of the coupled background error covariance $\mathbf{B}$ is clearly important for the dual DA formalism as is evident from the fact that the analysis equation projects the coupled system increments, $\delta\mathbf{x}$, onto the range of $\mathbf{B}$:

$$\delta\mathbf{x} = \mathbf{B}\mathbf{H}^{\mathsf{T}}(\mathbf{H}\mathbf{B}\mathbf{H}^{\mathsf{T}} + \mathbf{R})^{-1}\delta\mathbf{y}. \tag{1}$$

Here $\mathbf{H}$ is the (linearized) observation operator represented by an $l \times N$ matrix, with N and l being the dimension of the coupled state vector and the total number of observations in both fluids respectively, $\mathbf{R}$ is an $l \times l$ observation error covariance matrix, and $\delta\mathbf{y}$ is the innovation vector, containing concatenated vectors of innovations in the in the atmosphere $\delta\mathbf{y}_a \in \mathbb{R}^n$ and the ocean $\delta\mathbf{y}_o \in \mathbb{R}^m$ with $l = n + m$. In the following, we will focus on approximating a coupled solution $\widehat{\delta\mathbf{y}} = (\mathbf{H}\mathbf{B}\mathbf{H}^{\mathsf{T}} + \mathbf{R})^{-1}\delta\mathbf{y}$ in the observational space. After computing $\widehat{\delta\mathbf{y}}$, it is projected to the model grid to produce the coupled increment $\delta\mathbf{x}$.

As mentioned earlier, part of the technical problems faced by operational centers in their transition to a fully coupled assimilation mode is related to modifying the action of the coupled observation space error covariance matrix $\mathbf{P} = \mathbf{H}\mathbf{B}\mathbf{H}^{\mathsf{T}} + \mathbf{R}$ on the innovation vector as well as to the related tuning of the preconditioned observation space system solver. The action of the observation system solver will be denoted as multiplication by $\mathbf{P}^{-1}$. To alleviate the computational burden of solving the entire system of equations

$$\mathbf{P}\widehat{\delta\mathbf{y}} = \delta\mathbf{y} \tag{2}$$

required for computing the increment in (1), Frolov et al (2016) proposed to represent of the system matrix $\mathbf{P}$ by two parts $\mathbf{P}_{Ao}$ and $\mathbf{P}_{Oa}$ shown by the dotted squares in Fig. 1. These matrices contain ocean-atmosphere covariances only within the thin active boundary layers of both fluids and operate on the vectors $\delta\mathbf{y}_{Ao}$, $\delta\mathbf{y}_{Oa}$ containing concatenations of the innovations in the atmosphere and oceanic boundary layer and vice versa. After solving (in parallel) the two systems of equations

$$\mathbf{P}_{Ao}\widehat{\delta\mathbf{y}}_{Ao} = \delta\mathbf{y}_{Ao} \tag{3}$$
$$\mathbf{P}_{Oa}\widehat{\delta\mathbf{y}}_{Oa} = \delta\mathbf{y}_{Oa}, \tag{4}$$

the resulting solution vectors $\widehat{\delta\mathbf{y}}_{Ao}$ and $\widehat{\delta\mathbf{y}}_{Oa}$ are projected to the coupled model grid to obtain an approximation to the coupled increment. This approach is based on the assumption that on the time scale of the assimilation window (1-3 days) $\mathbf{P}$ is well approximated by a "nearly block-diagonal matrix" because the ocean and atmosphere errors appear to be correlated only within thin boundary layers (shown in Figure 1 by darker gray/black colors), while error cross-correlations between the upper atmosphere and the deep ocean (white areas in Figure 1) can be neglected. Judging by the results of testing by Frolov et al (2016), this assumption appears to be valid in general within a high degree of accuracy (1-2%). However, in some cases exhibiting strong ocean-atmosphere interaction, such as deep ocean convection or hurricane formation and development,

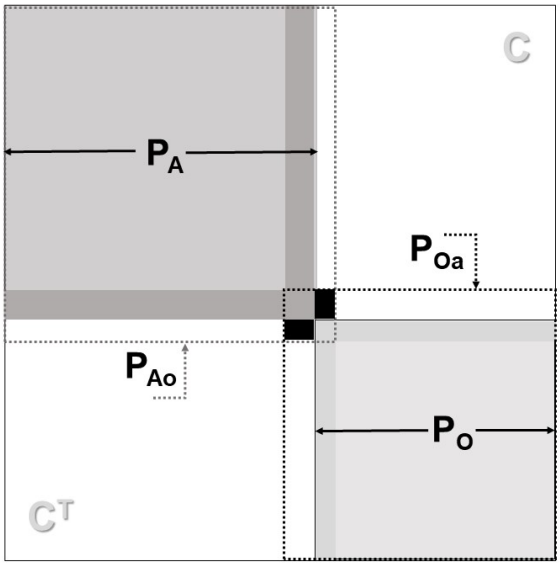

Figure 1. Partition of the system matrix. Capital letters in the subscripts denote the entire covariance matrices/vectors in the atmosphere (A) or ocean (O), while lower case letters denote the parts of the respective matrices/vectors corresponding to the atmospheric (a) and oceanic (o) boundary layers, where their coupling occurs. Matrix elements within the blocks denoted by $\mathbf{C}$ are assumed to be the largest in the black areas and close to zero in the white areas.

approximation accuracy could be low even on the time scale of the assimilation window, as the effective coupling may occupy boundary layers comparable with the total depths of the interacting fluids.

An apparent disadvantage of the method is the technical work caused by the necessity to modify existing uncoupled solvers that are required to solve equations (3–4). In the following, we show that these technical issues can be avoided by reducing the solution of the coupled problem (2) to a sequence of uncoupled problems.

3. Expansion of the strongly coupled DA problem using uncoupled solvers

As illustrated in Figure 1, the coupled system matrix $\mathbf{P}$ can be decomposed into the sum of two 2×2 block matrices:

$$\mathbf{P} = \begin{bmatrix} \mathbf{P}_A & \mathbf{0} \\ \mathbf{0} & \mathbf{P}_O \end{bmatrix} + \begin{bmatrix} \mathbf{0} & \mathbf{C} \\ \mathbf{C}^{\mathsf{T}} & \mathbf{0} \end{bmatrix} = \mathbf{P}_{\mathsf{unc}} + \mathbf{P}_{\mathsf{cc}}, \tag{5}$$

where $\mathbf{P}_A$ and $\mathbf{P}_O$ are respectively the $n \times n$ and $m \times m$ error covariances in the atmosphere and in the ocean, while $\mathbf{C}$ is the $n \times m$ ocean-atmosphere error cross-covariance matrix. The first term in the right-hand side of (5) is associated with the uncoupled system and will be denoted as $\mathbf{P}_{\mathsf{unc}}$. For the sake of clarity, we assume that $\mathbf{H}$ and $\mathbf{R}$ are conformably block diagonal themselves so that the second term, which we denote as $\mathbf{P}_{\mathsf{cc}}$, will involve only ocean-atmosphere cross-covariances. Extension of the method to the general non-block-diagonal $\mathbf{H}$ and $\mathbf{R}$ case is given in Appendix B. Equation (2) may be rearranged into

$$\widehat{\delta\mathbf{y}} = (-\mathbf{P}_{\mathsf{unc}}^{-1}\mathbf{P}_{\mathsf{cc}})\widehat{\delta\mathbf{y}} + \tilde{\mathbf{d}}_{\mathsf{unc}} \tag{6}$$

where $\tilde{\mathbf{d}}_{\mathsf{unc}} = \mathbf{P}_{\mathsf{unc}}^{-1}\delta\mathbf{y}$ is the solution that would be obtained in the absence of coupling, i.e., with $\mathbf{P}_{\mathsf{cc}} = \mathbf{0}$. Note that $\mathbf{P}_{\mathsf{unc}}^{-1}$ represents the action of the uncoupled solvers. The form of (6) suggests a fixed point recursion:

$$\widehat{\delta\mathbf{y}}^{k+1} = (-\mathbf{P}_{\mathrm{unc}}^{-1}\mathbf{P}_{\mathrm{cc}})\widehat{\delta\mathbf{y}}^{k} + \tilde{\mathbf{d}}_{\mathrm{unc}},$$

that will, given an initial vector $\widehat{\delta\mathbf{y}}^{0}$, determine a sequence of vectors, $\widehat{\delta\mathbf{y}}^{0}$, $\widehat{\delta\mathbf{y}}^{1}$, $\widehat{\delta\mathbf{y}}^{2}$.... Indeed, this is one formulation of the "block Jacobi method" (see, e.g., Axelsson (1994); Saad (2003)), a classical matrix iteration that, when convergent, will produce iterates $\widehat{\delta\mathbf{y}}^{k}$ that converge to the solution of (2) as $k \to \infty$. There are algorithmic advantages in reformulating this recursion as an incremental update:

$$\boxed{\begin{array}{l}\text{for} \quad k = 0, 1, 2, \ldots \text{(until converged)} \\ \quad \widehat{\delta\mathbf{y}}^{k+1} = \widehat{\delta\mathbf{y}}^{k} + \mathbf{s}^{k} \\ \quad \mathbf{r}^{k+1} = -\mathbf{P}_{\mathrm{cc}}\,\mathbf{s}^{k} \\ \quad \mathbf{s}^{k+1} = \mathbf{P}_{\mathrm{unc}}^{-1}\mathbf{r}^{k+1}\end{array}} \quad \begin{array}{l}\text{with} \quad \widehat{\delta\mathbf{y}}^{0} = \mathbf{0}, \\ \mathbf{s}^{0} = \tilde{\mathbf{d}}_{\mathrm{unc}}, \text{ and} \\ \mathbf{r}^{0} = \delta\mathbf{y}\end{array} \tag{7}$$

Practical implementation of (7) requires access to the uncoupled solvers associated with $\mathbf{P}_{\mathrm{unc}}^{-1}$ (these are readily available in existing systems) and the capacity for computing the action of $\mathbf{P}_{\mathrm{cc}}$ on a concatenated ocean-atmosphere innovation vector. This latter step should not be expensive because it represents multiplication by a sparse matrix $\mathbf{C}$ whose non-zero elements are localized in the vicinity of the interface between the interacting fluids (black rectangles in Fig. 1). Only three vector arrays are required: $\{\widehat{\delta\mathbf{y}}^{k}, \mathbf{r}^{k}, \mathbf{s}^{k}\}$, where $\widehat{\delta\mathbf{y}}^{k}$ is the approximate solution to (2); $\mathbf{r}^{k}$ is the *residual* vector associated with $\widehat{\delta\mathbf{y}}^{k}$ (mathematically equivalent to $\mathbf{r}^{k} = \delta\mathbf{y} - \mathbf{P}\widehat{\delta\mathbf{y}}^{k}$). This is a computationally accessible indicator of how well $\widehat{\delta\mathbf{y}}^{k}$ serves as a solution to (2) and as such may be examined to determine when the iteration (7) should be stopped.

Assuming that $\mathbf{P}$ is positive definite, the iteration described in (7) is convergent to the solution of (2). Convergence is a consequence of the spectral radius (magnitude of dominant eigenvalue) for the iteration matrix $\mathbf{M} = -\mathbf{P}_{\mathrm{unc}}^{-1}\mathbf{P}_{\mathrm{cc}}$ being strictly smaller than 1 (see e.g., Axelsson (1994)). The definition of $\mathbf{s}^{k}$, in (7) implies that $\mathbf{s}^{k} = \mathbf{M}^{k}\tilde{\mathbf{d}}_{\mathrm{unc}}$ and so, $\widehat{\delta\mathbf{y}}^{k} = \sum_{j=0}^{k}\mathbf{M}^{j}\tilde{\mathbf{d}}_{\mathrm{unc}}$, which is the kth partial sum of the expansion

$$\widehat{\delta\mathbf{y}} = \sum_{j=0}^{\infty}\mathbf{M}^{j}\tilde{\mathbf{d}}_{\mathrm{unc}}. \tag{8}$$

It is useful to note that on time scales of 1-3 days (which would be typical for the settings considered) the coupled solution differs from the uncoupled solution only within relatively thin boundary layers (Figure 1), and so few iterations are needed to achieve a solution accuracy within the uncertainty in specification of the system solver $\mathbf{P}^{-1}$. In terms of the expansion matrix this means that

$$\left|\sum_{k=1}^{\infty}\mathbf{M}^{k}\tilde{\mathbf{d}}_{\mathrm{unc}}\right| \ll |\tilde{\mathbf{d}}_{\mathrm{unc}}|, \tag{9}$$

i.e. the zeroth term (uncoupled solution) of the infinite expansion for $\widehat{\delta\mathbf{y}}$ given by eq. (8) dominates over other terms which provide relatively small corrections to $\tilde{\mathbf{d}}_{\mathrm{unc}}$. As a consequence, the accuracy of iterative approximations of $\delta\mathbf{y}$ depends on the magnitude of the projection of $\tilde{\mathbf{d}}_{\mathrm{unc}}$ on the slower converging eigenmodes of $\mathbf{M}$ with relatively large eigenvalues. These modes correspond to strong ocean-atmosphere coupling and are thus mostly responsible for larger corrections to $\tilde{\mathbf{d}}_{\mathrm{unc}}$ in the respective regions. If the uncoupled solution has a small projection on these modes (i.e. if strong coupling events simultaneously occur over small portion of the domain), the coupled solution would be reasonably well approximated by just a few iterations of (7), as appears to be the case in the experiments of Frolov et al (2016) performed in the Mediterranean basin. We assume that this property of the strongly coupled solution is likely to be valid in a global setting as well.

As mentioned earlier, in particular places (such as in the regions of deep convection near Greenland, or within hurricanes), convergence will be slower. On the other hand, it is in these regions the data are especially sparse and sometimes absent for purely technical reasons. So regions of strong ocean-atmosphere coupling account for only a minor part of the global data sets subject to operational assimilation, and, therefore will not break the general rule (9). The relationship (9) also indicates that the mean eigenvalue of $\mathbf{M}$ when averaged over the entire spectrum tends to be much smaller than 1, resulting in fast convergence of the Jacobi iterations. Results of the numerical experiments with an interface solver shown in Fig. 7 of Frolov et al (2016), as well as numerical experiments in Section 4 and analytic estimates in the Appendix A appear to support this notion.

There exists a large variety of strategies in literature to accelerate convergence, the most standard and popular being preconditioned conjugate gradient (PCG) iteration, using some variation on the block Jacobi step presented in (7) as a preconditioning step ("block diagonal preconditioning"). While PCG provides optimal acceleration in a certain sense, the resources required for a single step may increase substantially over what (7) requires because of the need to accumulate inner products between cycles (which principally adds overhead via required data motion). There are simpler alternatives to PCG that build on the same framework we have described above and involve no additional data motion, solver utilization, or intrusive recoding beyond what (7) requires. A major drawback for all of these alternatives, though, is that they require some type of *a priori* spectral information on $\mathbf{M}$ or on $\mathbf{P}$. We mention a few in passing and refer interested readers to Saad (2003) or Axelsson (2010) for a survey of related ideas.

In particular, polynomial acceleration provides a simple way of accelerating the iteration given in (7), while the variant known as the "Chebyshev semi-iterative method" (Golub et al. (1961)) can halve (or better) the number of iterations that (7) requires, without causing any significant change to the computation or communication costs per cycle. Other block iterative methods such as the Gauss-Seidel method and their relaxed versions such as Successive Overrelaxation (SOR) have similar advantages and similar drawbacks (Axelsson (1994)). Assessment of their utility mostly depends on the particular features of the DA systems subject to transition to the coupled regime.

4. Numerical test

To test the method, we conducted a series of Observation System Simulation Experiments (OSSEs). In these experiemnts, the ensemble of coupled ocean-atmosphere states was assumed to represent the true statistics of ocean-atmosphere interaction, which provided the true strongly coupled solution for a given set of simulated obeservations. The true solution was then approximated by the iterative solutions, the approximation errors were averaged over the sets of simulated observations, and represented as functions of the number of iterations.

4.1. *Ensemble data*

In the experiments, we used the ensemble of temperature profiles extracted from the CERA-20C coupled ensemble reanalysis described in Laloyaux et al (2018). The ensemble has $n_e = 25$

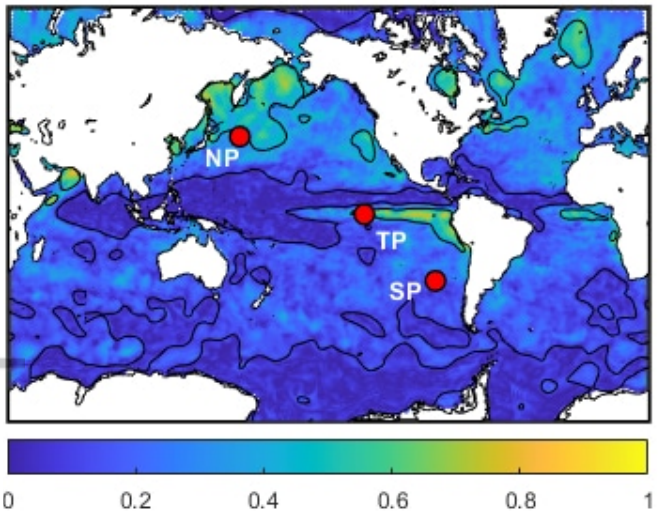

Figure 2. Correlation magnitude between SST and surface air temperature for August 2005 (similar to Figure 3c in Laloyaux et al (2018)). Locations of the three experimental sites are shown with red circles.

members generated by the ECMWF data assimilation using the hybrid DA technique of Bonavita et al (2016).

Locations of the temperature profiles in space (Figure 2) and time (August 31, 2005) represent three distinct coupling regimes between the ocean and atmosphere and include:

1. The Tropical Pacific (hereinafter TP): cold tongue is characterized by strong horizontal gradients of SST associated with Rossby instabilities along the equatorial upwelling front. Similar to other boundary currents (e.g. Gulf Stream or the Antarctic Circumpolar current) the SST perturbations are known to drive the variability and response of the lower atmospheric winds, temperatures, cloud cover and precipitation (Frenger et al (2013), Chelton et al (2004), Frolov et al (2021)). These processes translate to strong atmosphere-ocean correlations along the SST fronts.
2. Mid-latitude summer (NP): As the mixed layer depth shallows in the mid-latitude summer, the surface ocean starts to respond rapidly to perturbation in the wind stress (Feng et al (2016), Laloyaux et al (2018), Frolov et al (2021)), which causes increased correlations between the ocean surface and the atmosphere.
3. Mid-latitude winter (SP): As the ocean mixed layer deepens in mid-latitude winter, the surface ocean becomes less responsive to atmospheric perturbations, which translates to reduced correlations between the surface ocean and the atmosphere (Feng et al (2016), Laloyaux et al (2018)).

The temperature profiles' lengths were $N = 127 - 133$ points in the vertical, including 91 fixed pressure levels in the atmosphere and 36-42 levels in the ocean, depending of the total depth at a given location. The distribution of levels in the ocean-atmosphere column is given in Figure 3.

4.2. *Experiment setting*

The OSSEs were done by randomly selecting 30 observations locations in the vertical (see below for details), specifying an ensemble of innovations with prescribed statistics, and assuming that the CERA ensemble provides a realistic approximation to the true background error covariance matrix $\mathbf{B}$. The latter

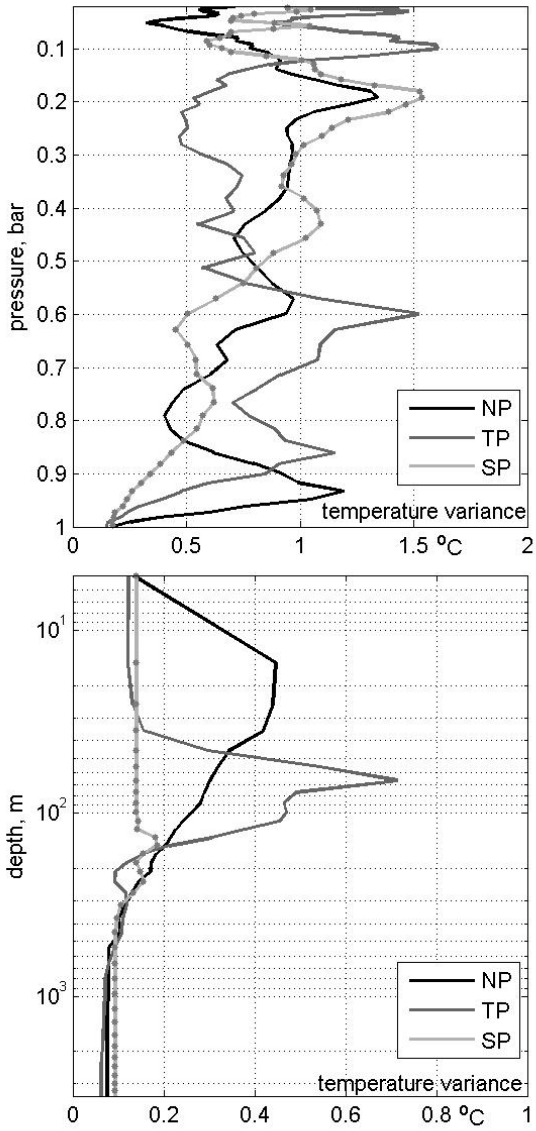

Figure 3. Background temperature rms error variances (°C) in the atmosphere (upper panel) and in the ocean (lower panel) used in the experiments. Model level locations are shown by dots on the SP profiles

was computed using the $N \times n_e$ ensemble matrix $\mathbf{X}$ of CERA temperature profiles by localizing the respective ensemble-based estimate:

$$\mathbf{B} = \mathbf{L} \circ \mathbf{X}'\mathbf{X}'^{\mathsf{T}}/(n_e - 1), \tag{10}$$

where $\mathbf{X}'$ is the deviation of $\mathbf{X}$ from the ensemble mean, $\mathbf{L}$ is the localization matrix and $\circ$ stands for the Schur product. To explore the impact of the localization scheme, we used two types of localization matrices. The first one was taken from Laloyaux et al (2018) who used the localization method of Mènètrier et al (2015a) (hereinafter denoted by $\mathbf{L}_M$). The second type of localization was based on the Gaspari-Cohn localization function (Gaspari and Cohn (1999)), denoted by $\mathbf{L}_{GC}$) with the half-width of 10 grid points. Both types of localization kernels are defined on the coupled ocean-atmosphere state vectors and use variable localization scale, because of the inhomogeneous grid spacing (Fig. 3). However, the $\mathbf{L}_M$ scheme exhibits much more variation of the localization weights, which at certain instances were significant at separations exceeding 30 grid points.

The OSSEs were done using the following constraints:

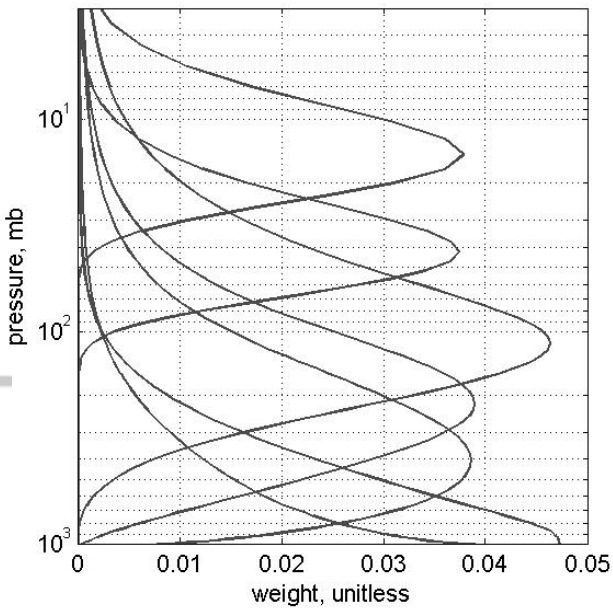

Figure 4. Radiance operators used in the experiments.

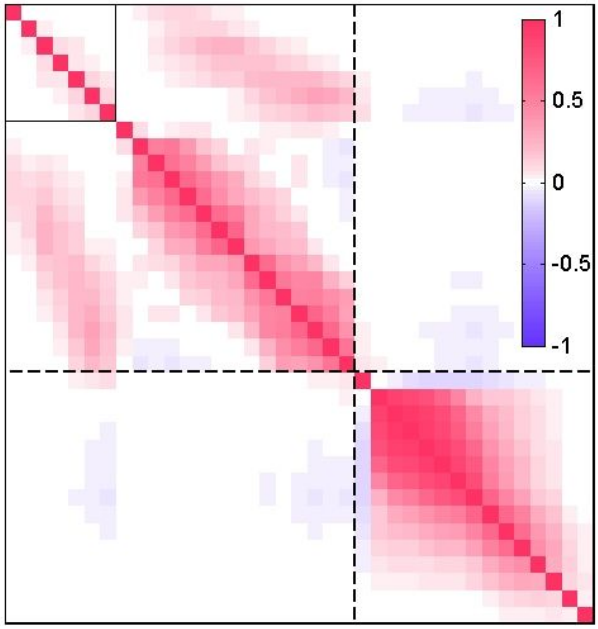

Figure 5. The system correlation matrix $\mathbf{C} = (\mathrm{diag}\mathbf{P})^{-1/2}\mathbf{P}(\mathrm{diag}\mathbf{P})^{-1/2}$ averaged of the 100 simulations of the observational system with Mènètrier et al (2015a) localization scheme. Dashed lines delineate the blocks for the atmospheric (upper left) and oceanic observations. Thin solid line within the atmospheric block outlines (non-local) radiance observations.

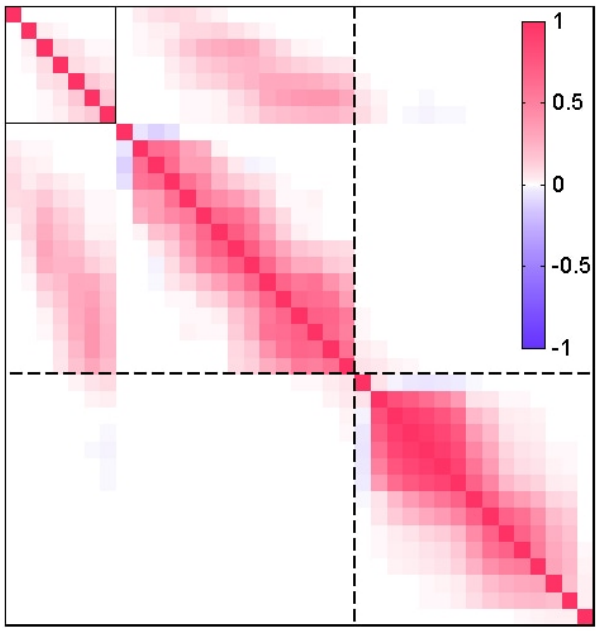

Figure 6. Same as in Figure 5, but for Gaspari-Cohn localization of the background error covariance.

1. The data available in an air-water column were $n = 22$ observations in the atmosphere and $m = 15$ observations in the ocean. In the atmosphere, there were 7 radiance observations, whose weighting functions are shown in Fig. 4 and $n' = 15$ *in situ* observations of the temperature profile, whose locations were randomly distributed over the 91 vertical levels. In the ocean, an SST observation was supplemented by 14 data points randomly distributed in the vertical within the range between 5 and 2000 m.
2. The background error variances were derived from the CERA ensemble and are shown in Fig. 3. It was assumed that the respective observation errors had a Gaussian distribution with zero mean and covariance $\mathbf{R} = 0.25\ \mathrm{diag}(\mathbf{B})$.
3. The innovation vector was generated by setting $\delta\mathbf{y} = \sqrt{\mathbf{HBH}^{\mathsf{T}} + \mathbf{R}}\nu$, where ν is a sample from the normal distribution.

For each OSSE, we computed the true solution $\delta\mathbf{x}_t = \mathbf{BH}^{\mathsf{T}}\widehat{\delta\mathbf{y}}_t$, and a set of $K = 5$ iterative approximations to $\delta\mathbf{x}_t$ using eq. (7). As mentioned above, the difference between the experiments within the ensemble was in random locations of $n' + m = 30$ *in situ* observations in the ocean and atmosphere, and in the random realizations of the innovation vectors. The total number of OSSEs for each of the three geographical locations was $J = 100$. The accuracy of solutions $\delta\mathbf{x}$ was quantified using the formula

$$e_j^k = \left[\frac{(\delta\mathbf{x}_j^k - \delta\mathbf{x}_t)^{\mathsf{T}}\mathbf{V}^{-1}(\delta\mathbf{x}_j^k - \delta\mathbf{x}_t)}{\delta\mathbf{x}_t^{\mathsf{T}}\mathbf{V}^{-1}\delta\mathbf{x}_t}\right]^{1/2} \quad 0 \le k \le K;\ 1 \le j \le J$$

where $\mathbf{V} = \mathrm{diag}\,\mathbf{B}$.

4.3. *Results*

A series of 1200 experiments in the setting described above was conducted using two types of localization with the fixed (37) number of observations. Figures 5 and 6 show the mean system matrices $\mathbf{P}$ averaged over 100 realizations of the simulated observations in the Tropical Pacific. It is seen that the structure of the off-diagonal blocks of $\mathbf{P}$ is generally consistent with the pattern exposed in Fig. 1: the matrix elements are dominated by near-zeros, while noticeable correlations occur in the vicinity of the ocean-atmosphere boundary layers. The largest correlations in the off-diagonal block are relatively small in magnitude ($0.1 - 0.15$). They are observed between the low-peaking radiances/surface atmospheric temperatures and the SST/

uppermost ocean temperature. Small negative correlations are also seen between the near-surface atmospheric temperatures and oceanic temperatures below the pycnocline (in the depth range 50-140m). It is noteworthy that the structure of the off diagonal blocks of $\mathbf{P}$ is much more pronounced in Figure 5 (with $\mathbf{L}_M$ localization): the ocean-atmosphere cross-correlations penetrate deeper in the troposphere and are almost 2 times larger in magnitude, reaching -0.1 at the altitudes of up to 900 HPa. We attribute this phenomenon to much larger localization scales of the $\mathbf{L}_M$ kernel.

Figure 7 shows reduction of the approximation error of the strongly coupled solution at the Tropical Pacific location. The convergence rate quantified by the average error reduction factor β per iteration is 5.43 for the $\mathbf{L}_M$ case and 5.68 for the Gaspari-Cohn localization. This is consistent with the relatively small norm of the off-diagonal blocks of $\mathbf{P}$ (Fig. 5) and the resulting spectral properties of the iteration matrix $\mathbf{M}$. In the experiments, we also computed the maximum eigenvalue σ of $\mathbf{M}$ (i.e., the spectral radius, $\rho(\mathbf{M})$), whose reciprocal provides a proxy to the mean reduction factor of the residual per iterate.

The results of experiments for all the three locations shown in Figure 2 are summarized in Table 1. The TP location exhibits the largest values of the mean initial approximation error e_0 (delivered by the uncoupled solutions), and $\rho(\mathbf{M})$, while the slowest convergence rate β was characterized by the approximately 5.5 times reduction of the approximation error per iterate (middle columns in table 1). We assume that this performance is still acceptable due to the relatively small error e_0. It is also evident that $\mathbf{L}_M$ localization produces, in general, larger uncoupled errors and somewhat slower convergence rates as compared to the Gaspari-Cohn localization, which is naturally explained by the larger localization scales in the $\mathbf{L}_M$ solutions.

Convergence rate of the proposed iterative correction algorithm largely depends on the projection of the innovation vector on the eigenmodes of $\mathbf{M}$ whose eigenvalues are close to 1 in magnitude. In the operational systems, the system matrices are mostly positive-definite and well-conditioned, leading to faster convergence. This property is maintained by removing redundancy in the assimilated data sets (e.g., replacing strongly correlated local observations by a single "super-observation"), considering "nearly orthogonal" bundles of the observation operators such as the one shown in Fig. 4, and careful localization/preconditioning of the background error covariances.

Region	NP		TP		SP	
localization	$\mathbf{L}_M$	$\mathbf{L}_{GC}$	$\mathbf{L}_M$	$\mathbf{L}_{GC}$	$\mathbf{L}_M$	$\mathbf{L}_{GC}$
e_0	.057	.017	.095	.038	.085	.008
$\rho(\mathbf{M})$	.118	.064	.187	.153	.130	.074
conv rate β	8.41	20.41	5.43	5.68	9.26	12.82

Table 1. Results of the OSSE experiments with two localization schemes in three different locations shown in Figure 2. The ensemble mean values over the 100 OSSEs are shown.

To explore the possibility of violating the condition $\mathbf{P} > 0$ by the system matrix, we conducted a series of additional experiments at the point (TP) of the slowest convergence. In the first series of experiments, we forced $\mathbf{B}$ to be positive semi-definite by forcefully setting a few of its smallest eigenvalues to zero. This procedure had no impact on the positive definite property of $\mathbf{P}$ primarily because the columns of $\mathbf{H}$ were linearly independent, while $\mathbf{R}$ was a diagonal matrix with a fairly small (less than 40) condition number. At the same time we did observe that the convergence shown in Fig. 7 slowed down, but not substantially:

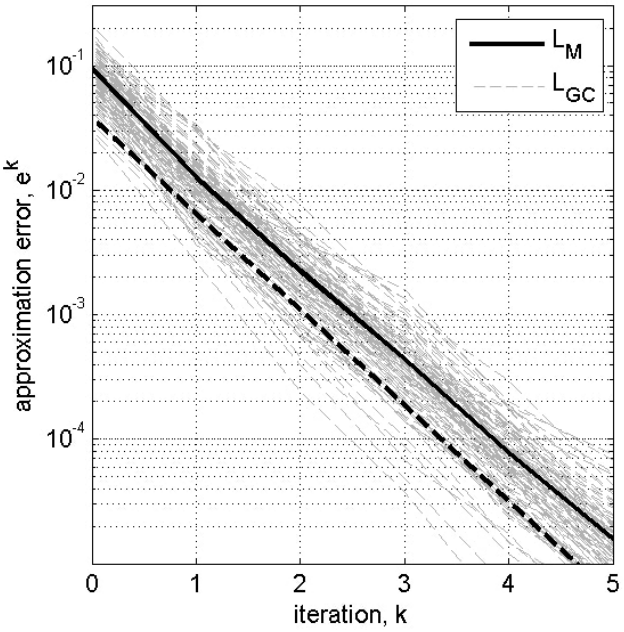

Figure 7. The approximation error of the strongly coupled solution as a function of the iteration number (eq. 9) with $\mathbf{L}_M$ localization in the Tropical Pacific. The thick solid line is the average over the ensemble of 100 OSSE experiments (shown by the dashed gray lines). Zeroth iteration corresponds to the error of approximation of the coupled solution by the uncoupled one ($e_0 = 10\%$). Thick dashed line shows the mean approximation error at the same location but with Gaspari-Cohn localization of the background error covariance.

even when half of the smallest eigenvalues of $\mathbf{B}$ were set to zero, the relative departure of $\mathbf{B}$ from its original form did not exceed 1%, while the values of β with both localization schemes experienced a decrease of only 1-5%. In the second series of experiments, we decreased the ratio $\gamma = 0.25$ of the observation-to-background error variances described in Section 4.2 down to 0.01, while keeping $\mathbf{B}$ positive semi-definite. This reduction had larger impact on the convergence rate, reducing β to 3.03 in the worst-case scenario ($\mathbf{L}_M$ localization, $\gamma = 0.01$ and half of the smallest eigenvalues of $\mathbf{B}$ set to zero). However, even in this case we assume that the value of β was still acceptable as it delivered a triple reduction of the uncoupled error (from 18% to 6%) after a single correction.

Convergence properties of the proposed correction scheme could be further improved by upgrading the method along the lines discussed in Section 3. The practical utility of such upgrades largely depends on the particular features of the DA systems being transitioned to the coupled regime.

5. Discussion

This study proposes an option for the development of operational strongly coupled DA systems using the uncoupled DA systems as a starting point. The approach employs already existing uncoupled solvers to build consecutive approximations to the strongly coupled solution. The only additional ingredient required is the development of the linear operator $\mathbf{P}_{cc}$ which couples the inputs to the existing uncoupled solvers. Testing the approach in a simplified setting with the CERA ensemble has shown that the proposed method requires less than 3 iterations to obtain a reasonable approximation to the strongly coupled solution.

Similar to the approach of Frolov et al (2016), the proposed formulation may require specification of the boundary layer thickness (coupled localization scales) as an external parameter in the code for applying $\mathbf{P}_{cc}$ to an observation vector. This parameter controls the number of non-zero elements in $\mathbf{P}_{cc}$ and can, in principle, be specified as a 2d field diagnostically computed from the background solution. One may think of the adaptive strategies in the specification of this field during the iterative process.

The proposed block matrix approach to the coupled assimilation problem can be easily generalized for the arbitrary number of coupled models in both dual and primal formulations (Appendix B) provided that the respective covariance matrices are positive definite. In real applications with the uncoupled solver matrix sizes exceeding $10^6 \times 10^6$, only a limited number of iterations (usually less than a hundred) are performed to reduce the magnitude of the residual to an acceptable level. Consequently, the respective uncoupled solutions have non-zero projections on the eigenvectors of $\mathbf{P}_{unc}$ spanning the tail of its spectrum, thus implicitly violating the positive-definite property of the covariance matrices. Experiments in Section 4.3 indicate that this "implicit semi-positive definiteness" of the block-diagonal matrices has a minor effect on the convergence properties of the method. More important is the magnitude of the projection of the uncoupled solution on the eigenvectors of $\mathbf{M}$ whose eigenvalues are close to 1 in magnitude.

It is also remarkable that the number of non-zero eigenvalues of $\mathbf{M}$ is directly proportional to the partition parameter $\alpha = \min(n/m, m/n)$ (see Appendix A). Thus, in the case when observations in one of the coupled fluids are relatively sparse ($\alpha \to 0$) the convergence rate of the coupled solution will be defined by the relatively small number of eigenvalues. Note that in the limiting case $\alpha = 0$, increments in the unobserved fluid will still be affected by observations in its counterpart through the cross-correlations of the background error covariance matrix $\mathbf{B}$. In that respect, success of the coupled DA approach strongly depends on the accurate definition of $\mathbf{B}$ from the ensemble run. Given the limited ensemble size, the coupling efficiency largely depends on the localization method applied to the cross-fluid covariance derived from the ensemble, which requires further research. In particular, Frolov et al (2016) show that in the presence of poorly known error covariances, the interface solver can be configured to produce a more accurate solution than an exhaustive solver due to the ability to tune the atmosphere and ocean localization separately. Other studies have produced similar findings. In that respect, one could also think of combining the adaptive localization technique of Mènètrier and Auligne (2015) employed by Laloyaux et al (2018) with a more traditional static coupled localization method used by Frolov et al (2016).

Fine-tuning of the localization matrix is also important, as it will bring more realism in the adaptive description of spatially variable boundary layer thickness, which defines the computational efficiency of the iterative uncoupled approach and the approach of Frolov et al (2016)). As an example, Laloyaux et al (2018) who utilized the scheme of Mènètrier et al (2015a) observed much deeper (up to 300 m) vertical localization scales in the mid-latitude ocean as compared to the tropics. One may expect that regions with thicker boundary layers may correspond to larger eigenvalues of $\mathbf{M}$ while the respective eigenvectors will have concentrated support in these regions. So in the extreme cases, such as developing hurricanes, the global convergence of the iterative solver will tend to be slower in these regions, because the uncoupled innovations would have larger projections on the respective eigenvectors.

Despite these problems, convergence of the solver in a global setting could be much faster, primarily because strong ocean-atmosphere interactions on the time scales of a few days occupy just a small portion of the globe. More accurate forecasts of such localized events could be performed using specialized regional models with strongly coupled assimilation schemes without the block matrix iterates and the boundary layer approximation. It should be also noted, that numerical experiments of Frolov et al (2016) with the system of intermediate complexity demonstrated high accuracy of the boundary layer approximation, giving some grounds to conduct more comprehensive tests with the proposed iterative approach. These tests are currently underway with the global coupled ensemble developed by the Naval Research Laboratory.

Acknowledgements

This study was supported by Office of Naval Research project ESPC Coupled Data Assimilation S20-ESPC-04. Prof. C. Beattie was supported by the NSF grants DMS-1923221 and DMS-1819110.

Appendix A: Estimating convergence rates with coupled observations

Let $\mathbf{y}_o$ and $\mathbf{y}_a$ be the vectors of unbiased oceanic and atmospheric innovations of dimension m and n, respectively. Without loss of generality, suppose $n \geq m$ and introduce ocean-atmosphere coupling taking the form $\mathbf{y}_o = \mathbf{Q}\mathbf{y}_a + \mathbf{y}'_o$, where $\mathbf{y}'_o$ is the "uncoupled" constituent of $\mathbf{y}_o$ and $\mathbf{Q}$ is an arbitrary $m \times n$ coupling matrix. Then the ocean-atmosphere observation space error covariance matrix $\mathbf{P}$ is parameterized by the three matrices $\mathbf{P}_o = \langle \mathbf{y}'_o \mathbf{y}'^{\mathsf{T}}_o \rangle$, $\mathbf{P}_a = \langle \mathbf{y}_a \mathbf{y}^{\mathsf{T}}_a \rangle$, and $\mathbf{Q}$ in the following manner:

$$\mathbf{P} = \begin{bmatrix} \mathbf{P}_a & \mathbf{P}_a\mathbf{Q}^{\mathsf{T}} \\ \mathbf{Q}\mathbf{P}_a & \mathbf{P}_{ao} \end{bmatrix} \tag{11}$$

where $\mathbf{P}_{ao} = \mathbf{Q}\mathbf{P}_a\mathbf{Q}^{\mathsf{T}} + \mathbf{P}_o$.

Splitting in (eq. 5) is now represented by

$$\mathbf{P} = \mathbf{P}_{unc} + \mathbf{P}_{cc} = \begin{bmatrix} \mathbf{P}_a & \mathbf{0} \\ \mathbf{0} & \mathbf{P}_{ao} \end{bmatrix} + \begin{bmatrix} \mathbf{0} & \mathbf{P}_a\mathbf{Q}^{\mathsf{T}} \\ \mathbf{Q}\mathbf{P}_a & \mathbf{0} \end{bmatrix}, \tag{12}$$

and yields the following representation of the expansion operator $\mathbf{M} = -\mathbf{P}^{-1}_{unc}\mathbf{P}_{cc}$:

$$\mathbf{M} = \begin{bmatrix} \mathbf{0} & -\mathbf{Q}^{\mathsf{T}} \\ -\mathbf{P}^{-1}_{ao}\mathbf{Q}\mathbf{P}_a & \mathbf{0} \end{bmatrix}. \tag{13}$$

whose eigenvalues σ are defined by the characteristic equation:

$$\det(\mathbf{M} - \sigma\mathbf{I}_{m+n}) = (-1)^{n+m} \det \begin{bmatrix} \sigma\mathbf{I}_n & \mathbf{Q}^{\mathsf{T}} \\ \mathbf{P}^{-1}_{ao}\mathbf{Q}\mathbf{P}_a & \sigma\mathbf{I}_m \end{bmatrix} = 0 \tag{14}$$

where $\mathbf{I}_p$ denotes a $p \times p$ identity matrix. (14) can be rewritten as:

$$(-\sigma)^{n-m} \frac{\det\left[\mathbf{Q}\mathbf{P}_a\mathbf{Q}^{\mathsf{T}} - \sigma^2(\mathbf{Q}\mathbf{P}_a\mathbf{Q}^{\mathsf{T}} + \mathbf{P}_o)\right]}{\det(\mathbf{Q}\mathbf{P}_a\mathbf{Q}^{\mathsf{T}} + \mathbf{P}_o)} = 0. \tag{15}$$

As a consequence, $\mathbf{M}$ will have zero as an eigenvalue of multiplicity at least $n - m$ and in cases of sparse observations in one of the fluids, say $n \gg m$, the number of modes contributing to the correction of the innovation vector will be comparatively small.

The remaining $2m$ nonzero eigenvalues are the $\pm$ square roots of the eigenvalues σ^2 of the generalized eigenvalue problem:

$$\mathbf{Q}\mathbf{P}_a\mathbf{Q}^{\mathsf{T}}\mathbf{x} = \sigma^2(\mathbf{Q}\mathbf{P}_a\mathbf{Q}^{\mathsf{T}} + \mathbf{P}_o)\mathbf{x}, \tag{16}$$

From (16) it is evident that $\sigma^2 < 1$ because $\mathbf{x}^{\mathsf{T}}\mathbf{P}_o\mathbf{x} > 0 \quad \forall \mathbf{x} \neq 0$.

The eigenvalue problem (16) provides some insight to the factors governing the rate of convergence of the series (8). Taking into account that $\sigma^2 < 1$ in (16), the generalized eigenvalue problem (16) may be rearranged to obtain

$$\mathbf{Q}\mathbf{P}_a\mathbf{Q}^{\mathsf{T}}\mathbf{x} = \lambda\, \mathbf{P}_o\mathbf{x}, \quad \text{with} \quad \lambda = \frac{\sigma^2}{1-\sigma^2} \tag{17}$$

The eigenvalues $\lambda_{max} = \lambda_1 \geq \lambda_2 \geq \ldots$ of (17) are all real and non-negative and relate to the (nonzero) eigenvalues of $\mathbf{M}$ as $\sigma_{\pm k} = \pm\sqrt{\lambda_k/(1+\lambda_k)}$. Notice that any upper bound to the largest eigenvalue of (17): $\widehat{\rho} \geq \lambda_{max}$ induces a corresponding upper bound on the spectral radius of $\mathbf{M}$:

$$\rho(\mathbf{M}) = \sqrt{\frac{\lambda_{max}}{1+\lambda_{max}}} \leq \sqrt{\frac{\widehat{\rho}}{1+\widehat{\rho}}} < 1 \tag{18}$$

We can produce a simple *a priori* bound by employing spectral matrix norms and eq. (17):

$$\begin{aligned}\lambda_{max}(\mathbf{P}_o^{-1}\mathbf{Q}\mathbf{P}_a\mathbf{Q}^T) &\equiv \|\mathbf{P}_o^{-1/2}\mathbf{Q}\mathbf{P}_a\mathbf{Q}^T\mathbf{P}_o^{-1/2}\| \\ &= \|\mathbf{P}_o^{-1/2}\mathbf{Q}\mathbf{P}_a^{1/2}\|^2 \leq C\|\mathbf{Q}\|^2 = \widehat{\rho},\end{aligned}$$

where $C = \|\mathbf{P}_o^{-1}\|\,\|\mathbf{P}_a\| = \lambda_{max}(\mathbf{P}_a)/\lambda_{min}(\mathbf{P}_o)$ is the "composite condition number" of the covariance matrices in the ocean and atmosphere, while $\|\mathbf{Q}\|^2$ is the square of the largest singular value ξ_{max} of the ocean-atmosphere coupling matrix $\mathbf{Q}$. As a consequence, we arrive at the following upper bound for the spectral radius:

$$\rho(\mathbf{M}) \leq \sqrt{\frac{C\xi_{max}^2}{1+C\xi_{max}^2}} < 1 \tag{19}$$

This estimate guarantees that the proposed iteration will converge with any ocean-atmosphere coupling matrix $\mathbf{Q}$, and suggests a rapid convergence rate can be anticipated if $\mathbf{Q}$ is "small", say if $C\xi_{max}^2 < 0.6$. These estimates are of more qualitative value, however, and are likely to be extremely conservative. Much more accurate *a posteriori* estimates of convergence rates can be obtained directly from calculating the dominant eigenvalue of (17). These are the estimates provided in the second line of Table 1.

Appendix B: Implementation in systems of operational complexity

Consider a set of K uncoupled operational systems with DA algorithms separately developed for each of them, and assume that these algorithms are based on the best linear unbiased estimates in either primal or dual formulation. This means that the unitless increments $\delta\tilde{\mathbf{x}}_k$ to the systems' states can be computed *in parallel* using either

$$\delta\tilde{\mathbf{x}}_k = (\tilde{\mathbf{H}}_k^{\mathsf{T}}\tilde{\mathbf{H}}_k + \mathbf{I})^{-1}\tilde{\mathbf{H}}_k^{\mathsf{T}}\delta\tilde{\mathbf{y}}_k, \quad k = 1, ..., K \tag{20}$$

for the primal formulation(s) in the range of $\mathbf{B}_k$, or

$$\delta\tilde{\mathbf{x}}_k = \tilde{\mathbf{H}}_k^{\mathsf{T}}(\tilde{\mathbf{H}}_k\tilde{\mathbf{H}}_k^{\mathsf{T}} + \mathbf{I})^{-1}\delta\tilde{\mathbf{y}}_k, \quad k = 1, ..., K \tag{21}$$

for the dual formulation(s). Here $\tilde{\mathbf{H}}_k = \mathbf{R}_k^{-1/2}\mathbf{H}_k\mathbf{B}_k^{1/2}$ is the (unitless) observation operator, $\mathbf{I}$ denote identity matrices of the respective sizes, while the systems' increments $\delta\mathbf{x}_k$ and innovations $\delta\mathbf{y}_k$ are related to their unitless counterparts via the relationships

$$\delta\mathbf{x}_k = \mathbf{B}_k^{1/2}\delta\tilde{\mathbf{x}}_k; \qquad \delta\mathbf{y}_k = \mathbf{R}_k^{1/2}\delta\tilde{\mathbf{y}}_k.$$

Transition to the coupled formulation implies (technically simple) concatenation of the state vectors and innovations and development of the codes for the (action of) coupled error covariance matrices $\mathbf{B} = \mathbf{B}_{\mathsf{u}} + \mathbf{B}_{\mathsf{c}}$, $\mathbf{R} = \mathbf{R}_{\mathsf{u}} + \mathbf{R}_{\mathsf{c}}$ and the observation operator $\tilde{\mathbf{H}} = \tilde{\mathbf{H}}_{\mathsf{u}} + \tilde{\mathbf{H}}_{\mathsf{c}}$, where the subscript $_{\mathsf{u}}$ denotes the uncoupled constituent (the block-diagonal part) of a matrix.

The proposed transition scheme relies on the availability of the codes for the block-diagonal solvers in eqns. (20-21) and on the observation that $K(K-1)/2$ off-diagonal blocks in the coupling matrices $\mathbf{B}_{\mathsf{c}}$, $\mathbf{R}_{\mathsf{c}}$, and $\mathbf{H}_{\mathsf{c}}$ in the operational systems are either zeros (for the non-interacting subsystems) or sparse.

Since in most geophysical applications $\mathbf{B}$, $\mathbf{R}$ and their diagonal blocks (uncoupled constituents) are positive-definite and $\tilde{\mathbf{H}}_k$ have full row rank, the solution of the coupled DA system $\delta\tilde{\mathbf{x}}$ could be obtained recursively (eq. 7) by applying the uncoupled system solvers to a sequence of the right-hand-side vectors. Using the notation of (20-21), the iterative process (7) can be formulated by replacing $\tilde{\mathbf{d}}_{\mathsf{unc}}$ by $\delta\tilde{\mathbf{y}}$ and setting

$$\begin{aligned}\mathbf{P}_{\mathsf{unc}} &= \tilde{\mathbf{H}}_{\mathsf{u}}^{\mathsf{T}}\tilde{\mathbf{H}}_{\mathsf{u}} + \mathbf{I} \\ \mathbf{P}_{\mathsf{cc}} &= (\tilde{\mathbf{H}}_{\mathsf{u}}^{\mathsf{T}}\tilde{\mathbf{H}}_{\mathsf{c}} + \tilde{\mathbf{H}}_{\mathsf{c}}^{\mathsf{T}}\tilde{\mathbf{H}}_{\mathsf{u}} + \tilde{\mathbf{H}}_{\mathsf{c}}^{\mathsf{T}}\tilde{\mathbf{H}}_{\mathsf{c}})\tilde{\mathbf{H}}^{\mathsf{T}}\tilde{\mathbf{H}}\end{aligned} \tag{22}$$

for the primal DA formulation, and

$$\begin{aligned}\mathbf{P}_{\mathsf{unc}} &= \tilde{\mathbf{H}}_{\mathsf{u}}\tilde{\mathbf{H}}_{\mathsf{u}}^{\mathsf{T}} + \mathbf{I} \\ \mathbf{P}_{\mathsf{cc}} &= \tilde{\mathbf{H}}_{\mathsf{u}}\tilde{\mathbf{H}}_{\mathsf{c}}^{\mathsf{T}} + \tilde{\mathbf{H}}_{\mathsf{c}}\tilde{\mathbf{H}}_{\mathsf{u}}^{\mathsf{T}} + \tilde{\mathbf{H}}_{\mathsf{c}}\tilde{\mathbf{H}}_{\mathsf{c}}^{\mathsf{T}}\end{aligned} \tag{23}$$

in the case of the dual formulation. Since the codes for $\mathbf{P}_{\mathsf{unc}}$ and its iterative inversion are already available, the only technical problem is development of the code simulating the action of the sparse matrix $\mathbf{P}_{\mathsf{cc}}$ on a data space vector obtained by concatenating the respective vectors of the system constituents.

Technically, the implementation of (22-23) can be done in many ways and could be adjusted for a particular DA system. As an option, instead of a separate development of the code for $\tilde{\mathbf{H}}_{\mathsf{c}}$ one can gradually develop (approximations to) $\tilde{\mathbf{H}}$ and use the identity $\tilde{\mathbf{H}}_{\mathsf{c}} = \tilde{\mathbf{H}} - \tilde{\mathbf{H}}_{\mathsf{u}}$ for computing the action of $\mathbf{P}_{\mathsf{cc}}$.

The proposed transition method should be viewed as an option which supports modularity in building the coupled DA system and enforces its parallelization capability. In particular, it does not require tuning and preconditioning of the coupled solver after adding a new DA component into the coupled system. In the 4dVar setting, the proposed technique appears to be more computationally intensive, as it requires additional adjoint model runs forced by the uncoupled and coupled components of the observation operator. These runs, however, can be executed in parallel, similar to the run of the uncoupled solver constituents.

References

Axelsson, O. (1994) Iterative solution methods, *Cambridge University Press*, ISBN 13: 9780521445245.

Axelsson, O. (2010) Milestones in the development of Iterative solution methods, *J. Electr. Comp. Engineering*, doi: 10.1155/2010/972794, 33pp.

Bauer, P., Thorpe, A.J. and Brunet, G. (2015) The quiet revolution of numerical weather prediction, *Nature*, 525, 47-55.

Bonavita, M., Holm, E., Isaksen, L.,and Fisher, M. (2016) the evolution of the ECMWF hybrid data assimilation system. *Quarterly Journal of the Royal Meteorological Society*, 142, 287-303.

Chelton, D. B., M. G. Schlax, M. H. Freilich, and R. F. Milliff, 2004: Satellite Measurements Reveal Persistent Small-Scale Features in Ocean Winds. Science (80-.)., https://doi.org/10.1126/science.1091901.

Feng, X., K. Haines, and E. de Boisseson, 2018: Coupling of surface air and sea surface temperatures in the CERA-20C reanalysis. Q. J. R. Meteorol. Soc., https://doi.org/10.1002/qj.3194.

Frenger, I., N. Gruber, R. Knutti, and M. Münnich, 2013: Imprint of Southern Ocean eddies on winds, clouds and rainfall. Nat. Geosci., 6, 608–612, https://doi.org/10.1038/ngeo1863.

Frolov, S, Bishop CH, Holt T, Cummings J, and Kuhl D. (2016) Facilitating strongly coupled ocean-atmosphere data assimilation with an interface solver. Mon. Weather Rev, 144: 4-19. https://doi.org/10.1175/MWR-D-15-0041.1.

Frolov S., Reynolds C., Alexander M., Flatau M., Barton N., Hogan P., Rowley C. Coupled ocean-atmosphere covariances in global ensemble simulations: Impact of an eddy-resolving ocean. Monthly Weather Review (under revision).

Gaspari, G., and S. E. Cohn (1999) Construction of correlation functions in two and three dimensions. Quart. J. Roy. Meteor. Soc., 125, 723–757, doi:10.1002/qj.49712555417.

Golub, Gene H., and Richard S. Varga. Chebyshev semi-iterative methods, successive overrelaxation iterative methods, and second order Richardson iterative methods. Numerische Mathematik 3.1 (1961): 147–156.

Laloyaux P, Balmaseda M, Dee D, Mogensen K, Janssen P. (2016) A coupled data assimilation system for climate reanalysis. *QJR Meteorol. Soc.*, 142(694): 65–78. https://doi.org/.

Laloyaux, P, Frolov S, Meńeťrier B, and Bonavita M, 2018. Implicit and explicit cross-correlations in coupled data assimilation, *QJR Meteorol. Soc.*, 144, 1851-1863. https://doi.org/10.1002/qj.3373.

Lea DJ, Mirouze I, Martin MJ, King RR, Hines A, Walters D,. Assessing a new coupled data assimilation system based on the Met Office coupled atmosphere and ocean sea ice model. *Monthly Weather Review* 2015; 143(11): 4678–4694.

Mènètrier and Auligne, T (2015) Optimized localization and hybridization of the ensemble-based covariances. *Mon. Weather Review*, 143, 3931-3947.

Mènètrier B, Montmerle, T, Michel, Y, and Berre, L (2015) Linear filtering of sample covariances for ensemble-based data assiimilation. Part I: optimality criteria and application to variance filtering and covariance localization. *Mon. Weather Review*, 143, 1622-1643.

Penny, S. G., S. Akella, M. Buehner, M. Chevallier, F. Counillon, C. Draper, S. Frolov, Y. Fujii, A. Karspeck, A. Kumar, P. Laloyaux, J-F. Mahfouf, M. Martin, M. Peña, P. de Rosnay, A. Subramanian, R. Tardif, and X. Wu. Coupled data assimilation for integrated Earth system analysis and prediction: goals, challenges and recommendations. *World Weather Research Programme Report 2017-3* 2017; 45pp.

Rabier F. Overview of global data assimilation developments in numerical weather-prediction centers. *Quarterly Journal of the Royal Meteorological Society*, 2005; 131(613): 3215–3233.

Saad, Yousef. Iterative methods for sparse linear systems. Society for Industrial and Applied Mathematics (SIAM), Philadelphia. 2003.

Sluka TC, Penny SG, Kalnay E, Miyoshi T. Assimilating atmospheric observations into the ocean using strongly coupled ensemble data assimilation. Geophysical Research Letters 2016; 43(2): 752–759.

Smith PJ, Fowler AM, Lawless AS. Exploring strategies for coupled 4D-Var data assimilation using an idealised atmosphere-ocean model. *Tellus A: Dynamic Meteorology and Oceanography* 2015; 67(1): 27025.

Smith PJ, Lawless AS, and Nichols N.K. (2017). Estimating forecast-error covariances for strongly coupled atmosphere-ocean 4D-Var data assimilation. *Monthly Weather Review*, 145, 4011–4035 27025.

Smith PJ, Lawless AS, Nichols NK. Treating sample covariances for use in strongly coupled atmosphere-ocean data assimilation. *Geophysical Research Letters* 2018; 45(1): 445–454. doi: 2017GL075534.

Wada A, Kunii M. The role of ocean-atmosphere interaction in typhoon Sinlaku (2008) using a regional coupled data assimilation system. *Journal of Geophysical Research: Oceans* 2017; 122(5): 3675–3695.

Zhang, S., and 12 coauthors, (2020) Coupled data assimilation and parameter estimation in coupled ocean-atmosphere models: a review. *Climate Dynamics*, 54, 5127–5144.

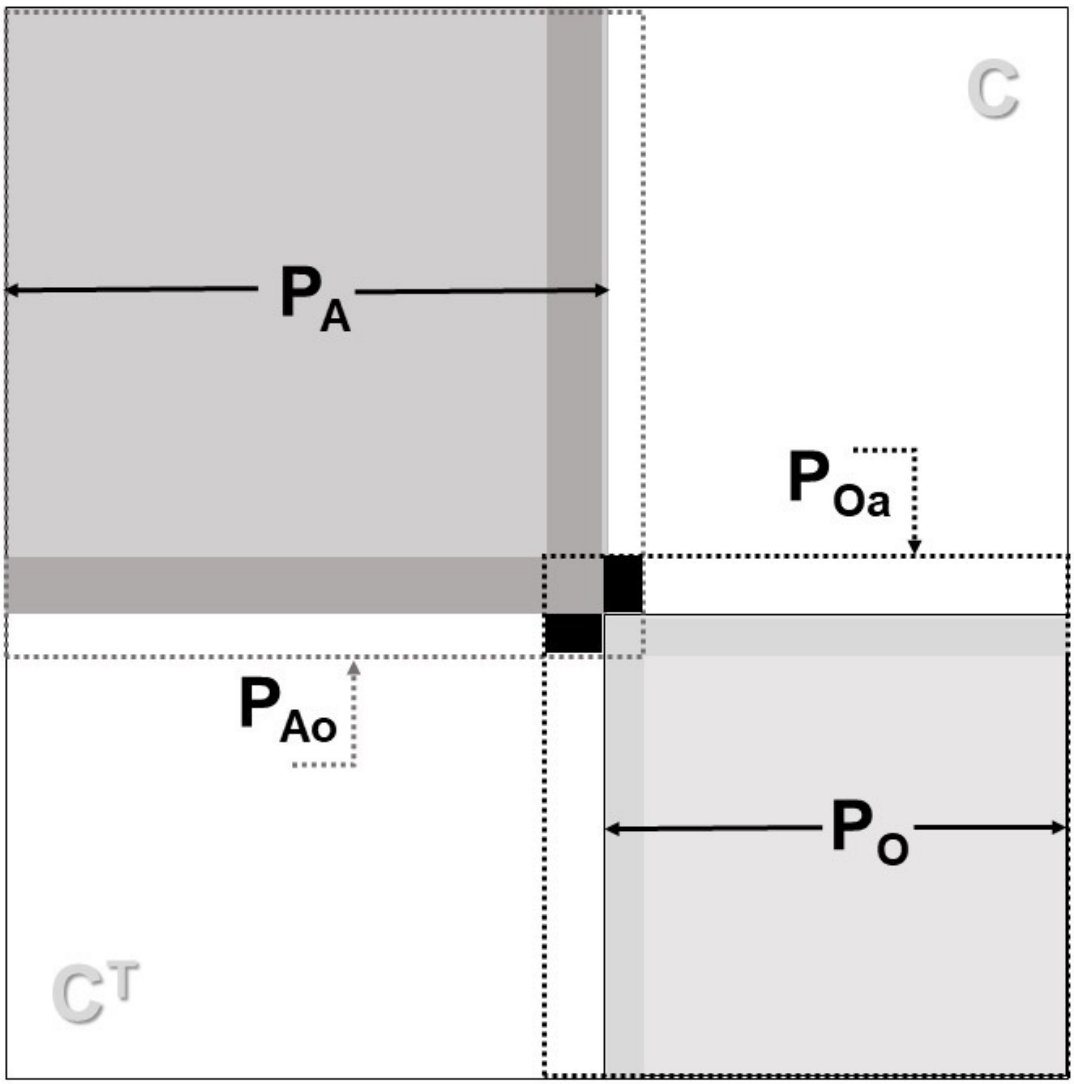

QJ_4047_fig1.jpg

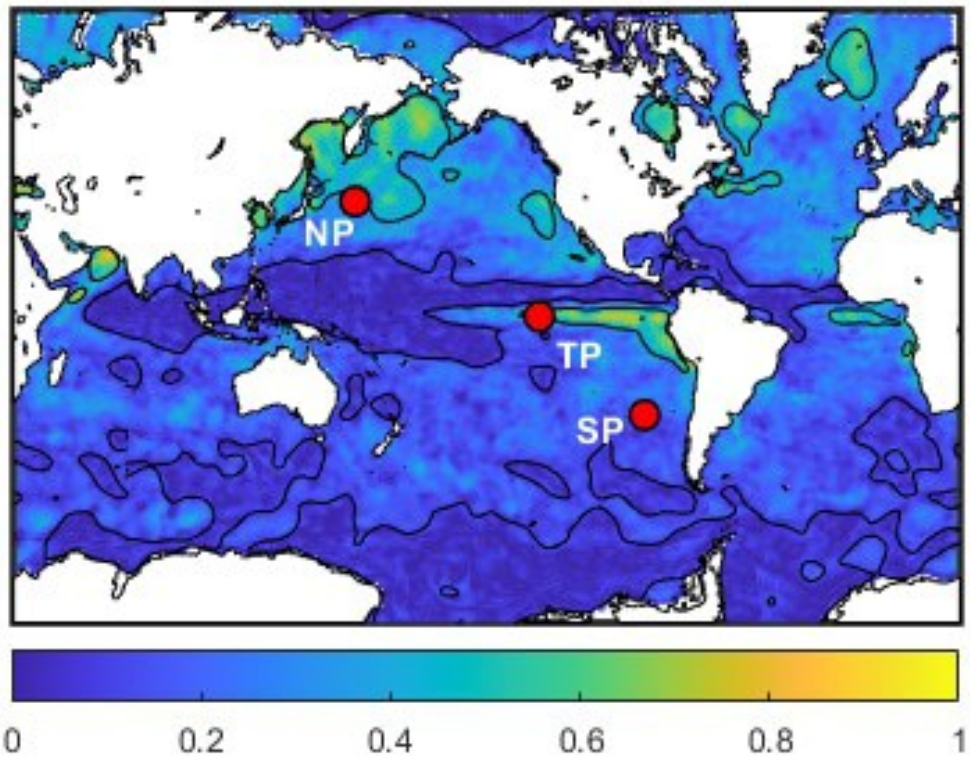

QJ_4047_fig2 (1).jpg

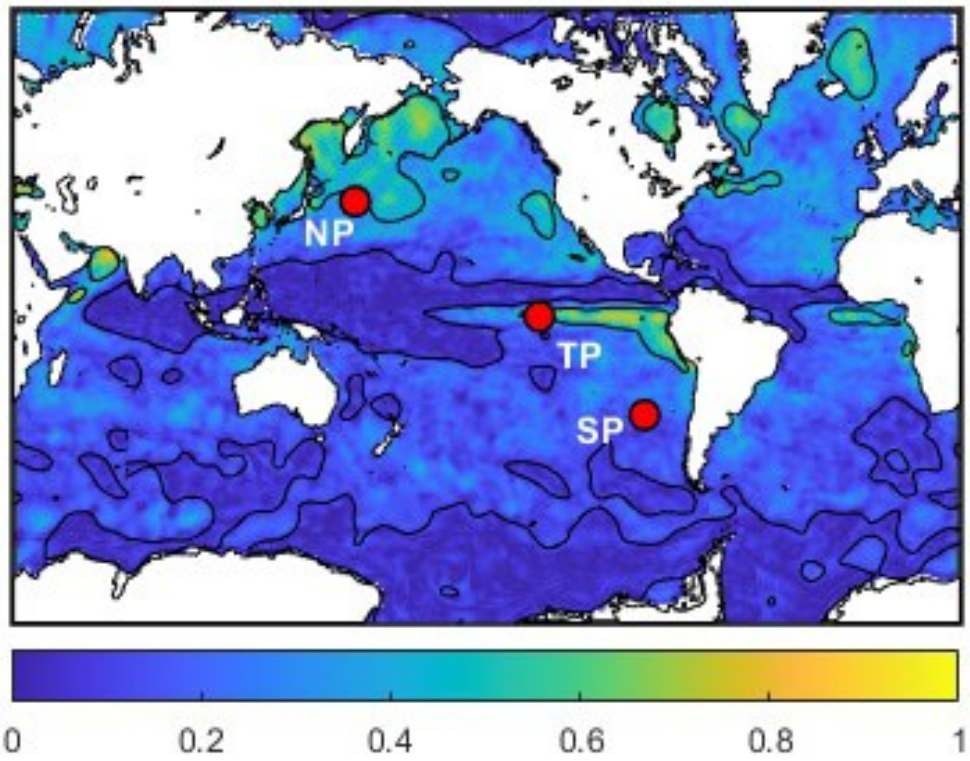

QJ_4047_fig2.jpg

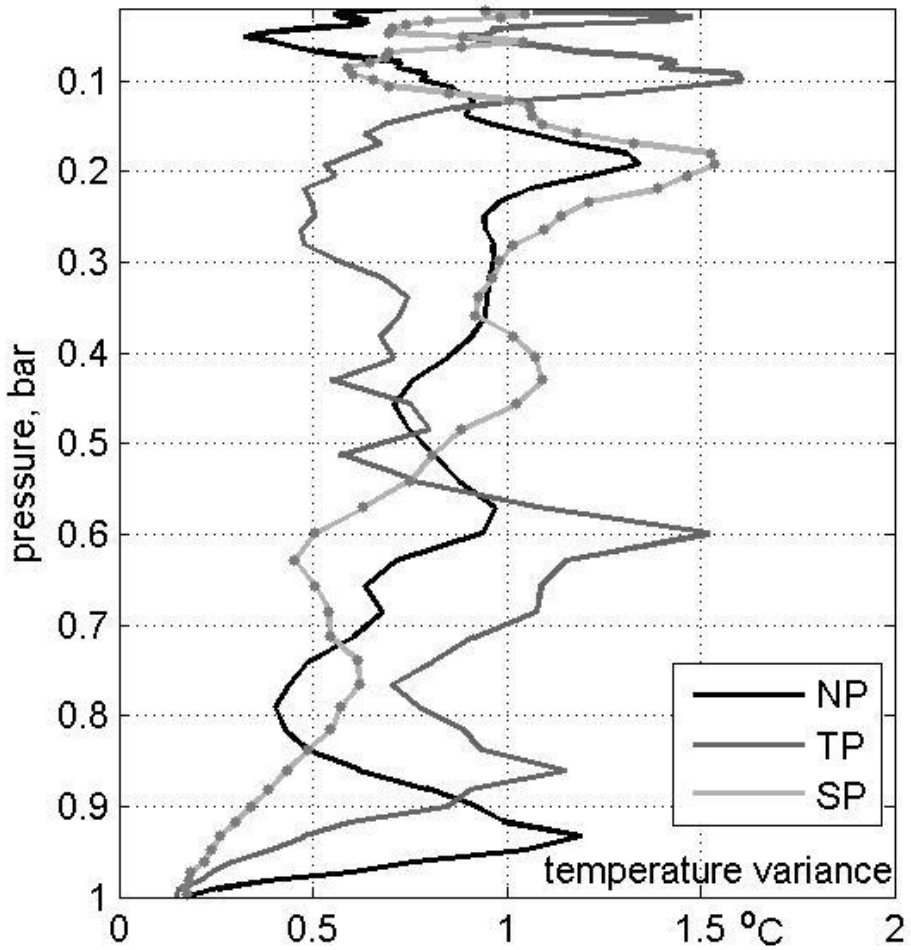

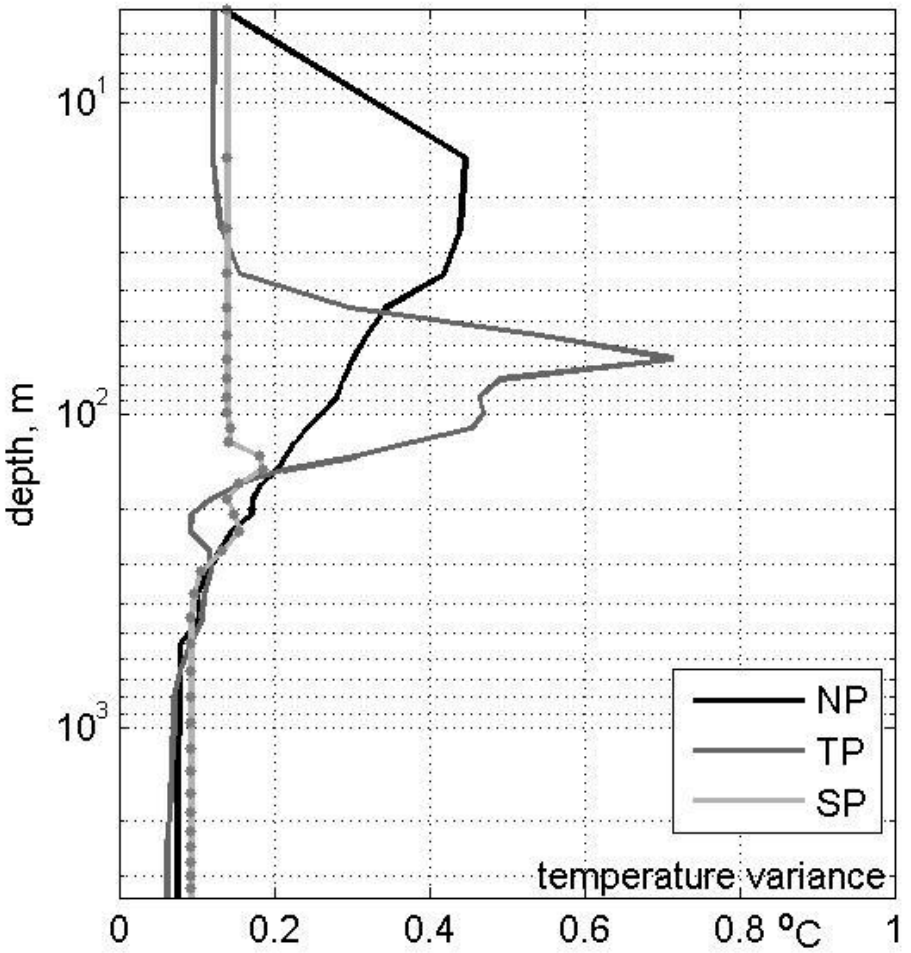

QJ_4047_fig3.jpg

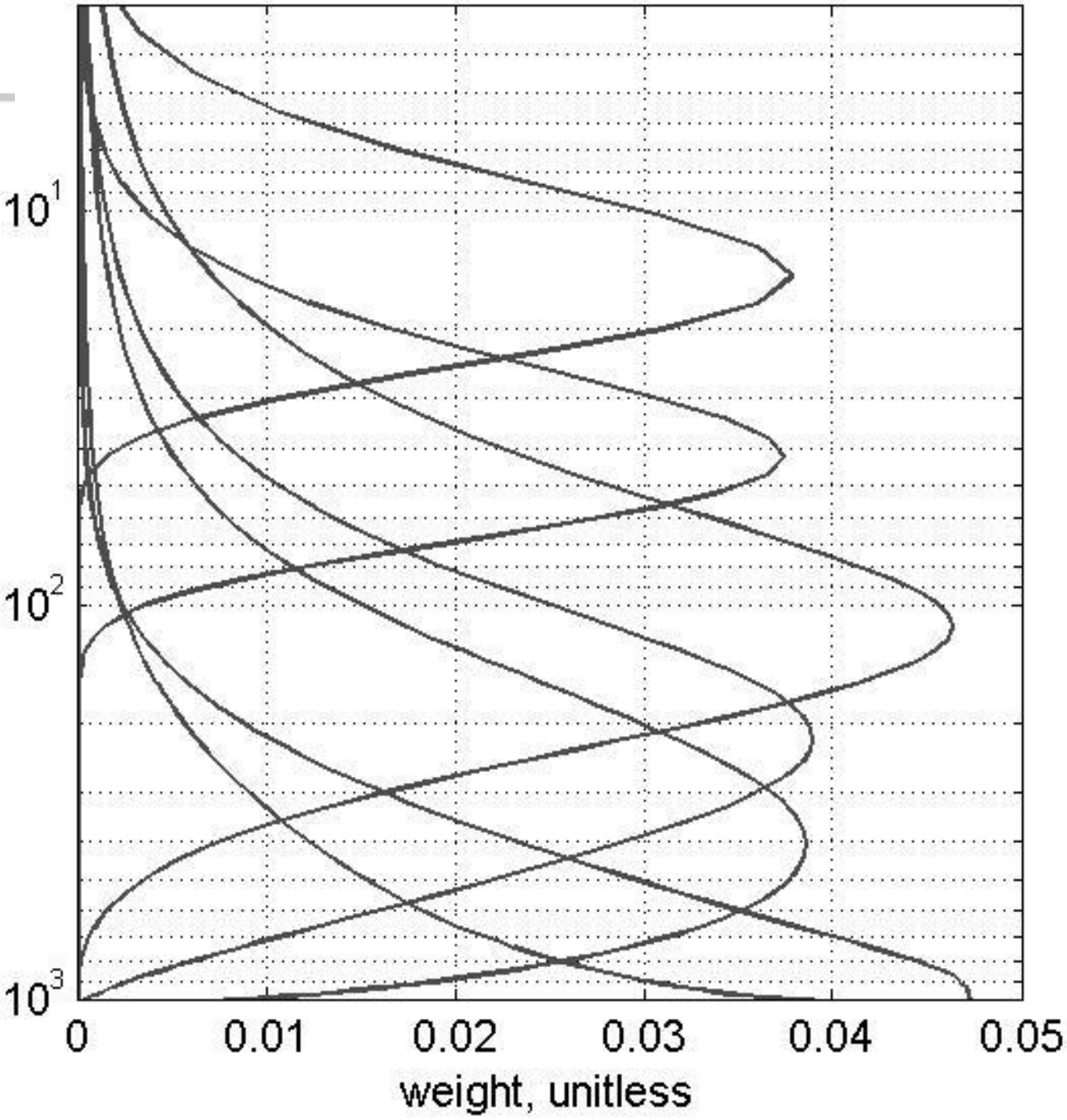

QJ_4047_fig4.jpg

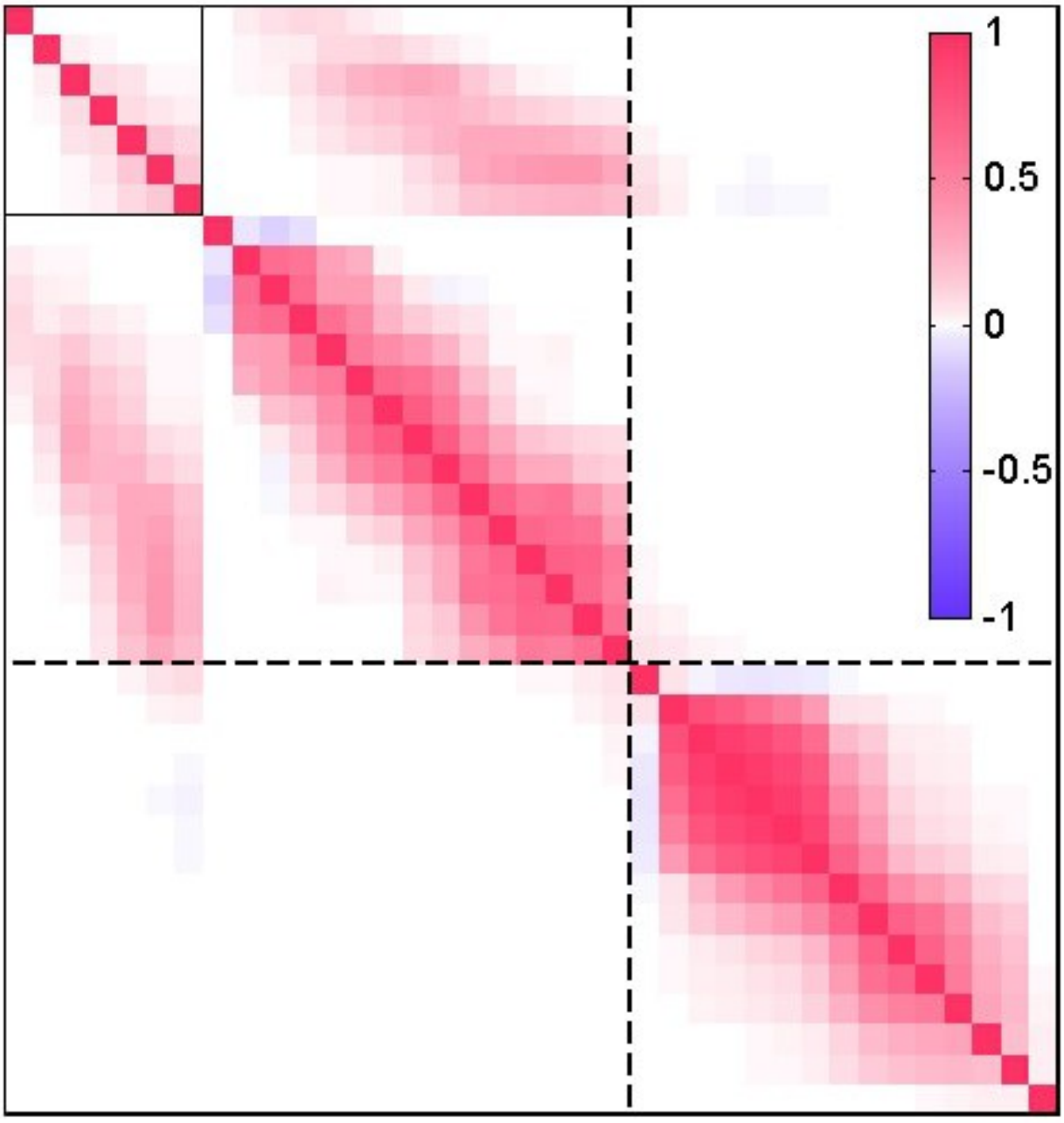

QJ_4047_fig5a.jpg

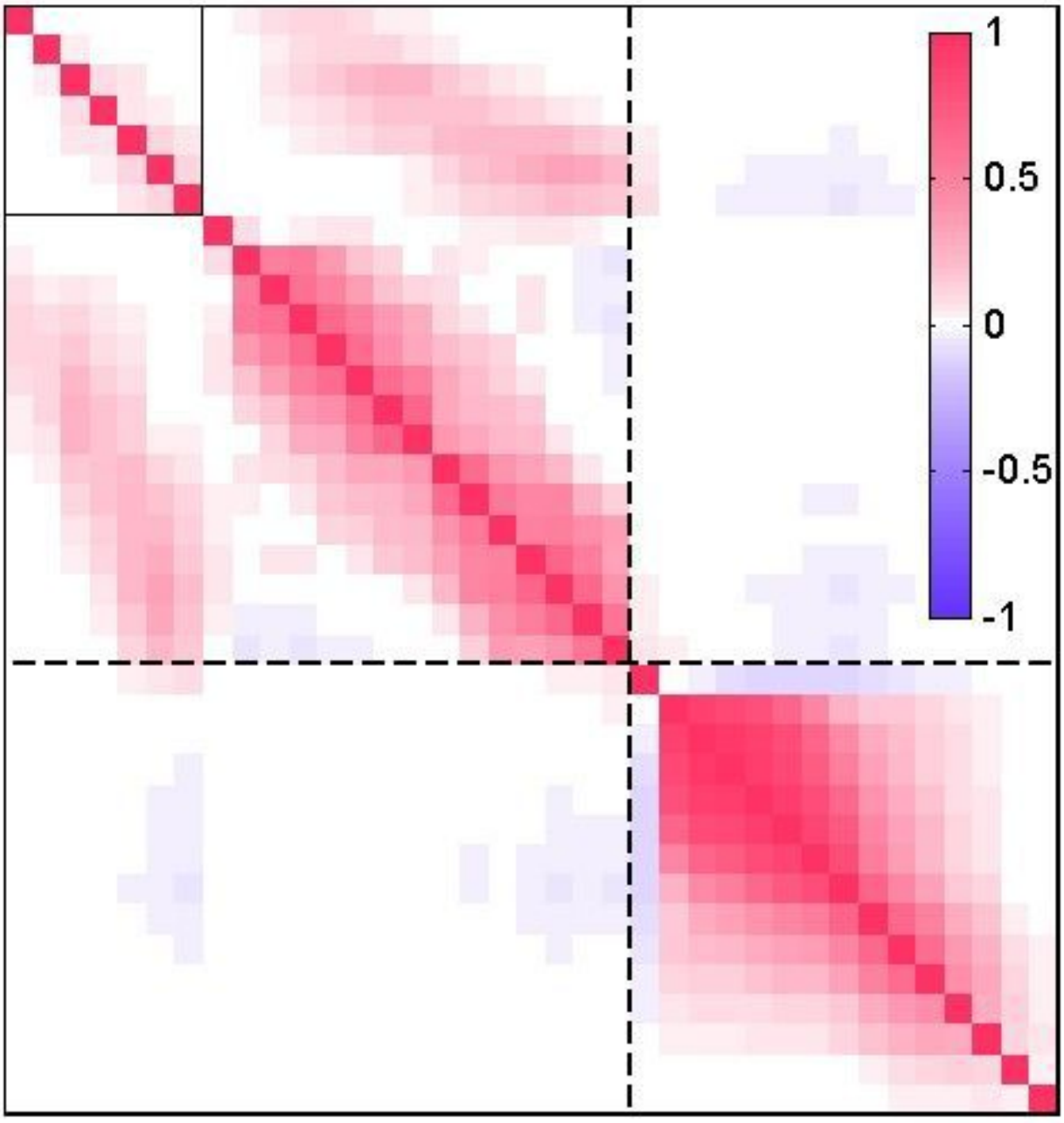

QJ_4047_fig5b.jpg

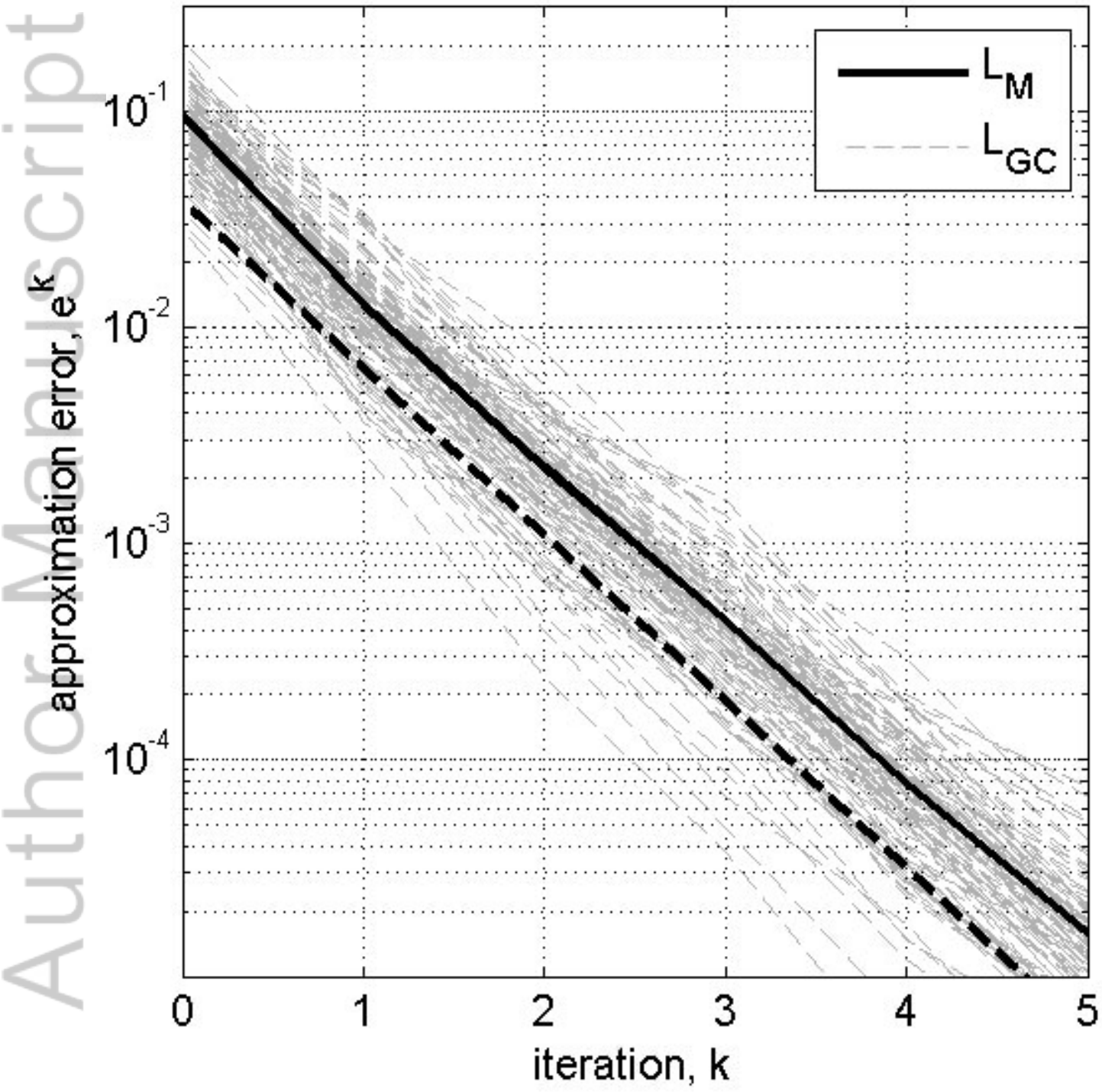

QJ_4047_fig6.jpg

On block iterative correction in strongly coupled data assimilation

M. Yaremchuk, C. Beattie, and S. Frolov

A method of recursive corrections is proposed for transitioning a set of uncoupled data assimilation systems to the strongly coupled formulation. The method is based on applying uncoupled solvers to sequence of coupled innovation vectors. Testing of the method with the CERA ensemble has shown its fast convergence: The approximation error of the strongly coupled solution drops 5-12 times per iteration depending on the location of the uncoupled solution subject to correction. Error reduction in the equatorial region of the Tropical Pacific is shown for two types of the localization kernels used to regularize the background error covariance.